Modelling the impact of aquaculture on early diagenetic processes in sea loch sediments

Daniele Brigolin[1,*], Roberto Pastres[1], Thomas D. Nickell[2], Chris J. Cromey[2], David R. Aguilera[3,4], Pierre Regnier[4,5]

[1]Department of Physical-Chemistry, University of Venice, Calle Larga S.Marta 2137, 30123 Venice, Italy

[2]Scottish Association for Marine Science, Dunstaffnage Marine Laboratory, Oban, Argyll PA37 1QA, UK

[3]DELTARES–TNO Built Environment and Geosciences, Dept. Groundwater quality, Princetonlaan 6, 3508 TA Utrecht, The Netherlands

[4]Department of Earth Sciences, Utrecht University, PO Box 80.021, 3508 TA Utrecht, The Netherlands

[5]Department of Earth and Environmental Sciences, CP 160/02, Université Libre de Bruxelles, 50 Av. F. D. Roosevelt, 1050 Brussels, Belgium

ABSTRACT: We present a novel approach for the simulation of the impacts of finfish aquaculture on sedimentary redox dynamics, based on the coupling of a fish farm waste deposition model (DEPO-MOD) and a knowledge-based reactive transport model (RTM) of early diagenesis. The integrated model was applied to a salmon fish farm located in a Scottish fjordic sealoch. The major diagenetic processes of the reaction network were first identified on the basis of literature information and historic data. Next, the organic carbon (OC) flux at a pristine site near the farm was estimated by fitting the vertical profiles of pore water and solid-state chemical species measured in the field. DEPOMOD was then used to predict the fluxes of OC due to the release of uneaten feed and faeces at various distances away from the farm. These fluxes were added to the background 'natural' fluxes and used as forcing functions for the RTM. Comparison of the simulated transient profiles with data collected at an impacted site revealed that the RTM model satisfactorily predicted the transient dynamics of the system. We discuss the use of the model for cost-effective environmental impact assessments, site selection and the optimization of husbandry practices.

KEY WORDS: RTM · DEPOMOD · Transient simulation · Loch Creran · Atlantic salmon · Benthic mineralization

INTRODUCTION

In the last decade, an increasing availability of surficial marine sediment datasets (including pore water and solid-phase chemistry data) stimulated the development of complex reaction–transport numerical models (RTM) of early diagenesis. These models offer a realistic representation of sediment biogeochemistry (e.g. Berg et al. 2003, Jourabchi et al. 2005, Thullner et al. 2005, Dale et al. 2008a) and are particularly suitable to simulate the vertical redox zonation coupled to the process of organic carbon (OC) oxidation, which is controlled by the availability of electron acceptors and

the Gibbs free energy associated with each metabolic pathway (Morel & Hering 1993). Moreover, the inclusion in the reaction network of re-oxidation processes of the reduced compounds produced during OC decomposition, as well as an accurate parameterization of diffusion and advection processes, enables the unravelling of sedimentary cycles and fluxes of redox-sensitive species (Thuller et al. 2007).

In addition, the recent development of user-friendly RTM codes (Regnier et al. 2002, 2003, Meysman et al. 2003a,b, Aguilera et al. 2005) has stimulated their use by an expanding scientific community. So far, however, early diagenetic numerical models were cali-

brated and/or tested by comparing model outputs at steady state with rate and concentration profiles observed in sediment (Thullner et al. 2005), whereas little work has been done on analysing the performances of these models in reproducing transient states, responding to time- or space-variable forcing conditions (e.g. Soetaert et al. 1996, Luff & Wallmann 2003, Dale et al. 2008a,b). From a methodological standpoint, this analysis can be regarded as a test for evaluating model robustness (sensu Gribble 2001), i.e. the ability of a system to continue to operate correctly across a wide range of operating conditions.

The application of early diagenesic models to predict changes in geochemical cycles due to anthropogenic perturbations are limited (e.g. Canavan et al. 2006). From this perspective, aquaculture site selection and monitoring represent potential new areas of application for RTMs. As the human population continues to expand, its reliance on farmed fish production as a source of protein is expected to increase (Naylor et al. 2000), in turn increasing the demand for aquatic resources. However, further sustainable development of aquaculture requires a careful assessment of their impacts, not only on pelagic ecosystems, but also on the benthic environment (Black 2001).

The need to forecast and monitor organic enrichment resulting from intensive marine aquaculture has led to the development of numerical models that provide an estimate of the response of the macrobenthic community to increased OC rain (Cromey et al. 2002a). In these models, the representation of the impact of aquaculture is based on empirical correlations between OC fluxes and macrobenthic community indices. However, recent work indicates that geochemical measures perform better than methods based on macrofaunal community analysis due to their cost-effectiveness; this has consequently increased the interest in early diagenesic studies (Hargrave et al. 1997, Wildish et al. 1999,

2001). In this regard, early diagenesic models could be used for the mechanistic simulation of the impacts of aquaculture on geochemical processes.

In the present work, a RTM of early diagenesis is applied to simulate the concentration profiles of redox species in sediments of a fjordic sea loch, at sites which were exposed to high OC fluxes from aquaculture. The model was first calibrated on pore water and sediment chemistry data collected at a pristine site under steady-state conditions. Secondly, the steady-state boundary conditions were perturbed by adding the fish farm-derived OC rain calculated by a particle-tracking model (DEPOMOD). Simulations were then performed to analyse the model response to the establishment of a new fish farm, and the transient profiles predicted by the model were compared with field data. The evaluation of the performance of the coupled models (DEPOMOD + RTM) was part of a larger EU research initiative focused on the development and testing of numerical models for aquaculture site selection and monitoring (www.ecasa.org.uk).

MATERIALS AND METHODS

Study site and field data description. Loch Creran is a fjordic sea loch located on the west coast of Scotland, with a surface area of approximately 10 km^2 and a maximum depth of 50 m (Fig. 1). The mean freshwater input is 286×10^6 m^3 yr^{-1}, and it has a relatively short flushing time of 3 d (Edwards & Sharples 1986). The loch has 4 main basins separated by narrow sills; the study site is located in a basin that is 9 km long and has a maximum depth of 49 m. The loch is relatively sheltered from wave action and has a freshwater runoff of 286×10^6 m^3 yr^{-1}. The important topographical features of Loch Creran are the 2 sills between the farm location and the fully marine Firth of Lorne. These sills have
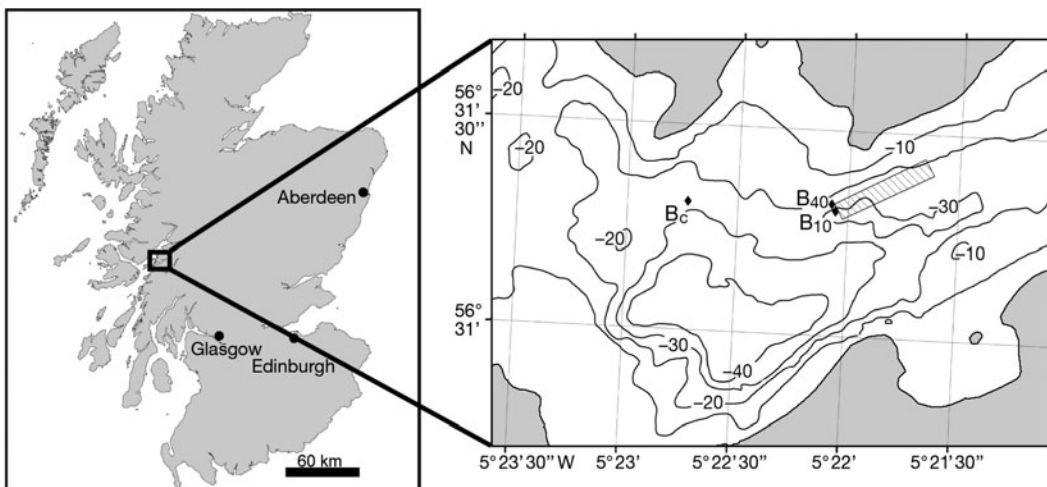

Fig. 1. Map of Scotland showing a portion of Loch Creran with sampling stations (♦), bathymetry (in m) and fish farm location (▨)

depths of 7 and 11 m, with deeper water on either side of them. Despite these topographic features, the site location is reasonably well flushed, with a flushing time of 3 d and a moderate current. The loch can be thermally and/or salinity stratified depending on season and rainfall. For a detailed description of the loch's morphology, cf. Tett & Wallis (1978) and Edwards & Sharples (1986). Salmon farming has been practiced in this loch for >10 yr, and fish cages are periodically re-sited to minimise environmental impacts and allow benthic recovery. The area sampled in the present study was impacted by organic deposits from a salmon farm that had been established in March 2006. The farm has a maximum consented biomass of 1.5×10^6 kg yr^{-1}. Atlantic salmon *Salmo salar* are reared in 6 circular net cages of 22 m diameter, with a net depth of 14 m.

A detailed biogeochemical survey was carried out at 3 stations, in order to calibrate/validate the early diagenesis model. Station location, cage arrangement and bathymetry of the area are depicted in Fig. 1. Samples were collected on 17 August 2006, approximately 6 mo after the establishment of the fish farm. Three stations were sampled: B_{10}, situated 10 m from the edge of the cage; B_{40}, away from the cage, but still within the depositional footprint; and B_c, a non-impacted control site. Samples were collected from RV 'Calanus' using a Bowers & Connelly megacorer (core i.d. = 100 mm; Barnett et al. 1984). Nickell et al. (2003) reported the results from a video survey, characterising this area of Loch Creran as soft and muddy sediments.

Cores were placed in stands and kept under running seawater until returned to the laboratory. The following day, each 10 cm long sediment core was sliced into 1 cm layers in a glove bag under nitrogen and maintained at 4°C, in order to obtain high resolution data for each chemical variable. Slices sub-sampled for OC and total phosphorous were kept frozen at −20°C; pore water was extracted by centrifuging slices obtained under nitrogen, and kept refrigerated (4°C) for analysis. Porosity was determined by weighing wet sediment, freeze drying and re-weighing. The spectrophotometric analysis of pore water ammonia was based on the standard Berthelot method adapted by O'Dell (1993). The analysis of total (inorganic and organic) phosphorus in the sediment was based on the classic molybdate/ascorbic acid and spectrophotometric method described by Strickland & Parsons (1972), with modification by Aspila et al. (1976). Organic carbon (CHN) samples were lyophilised, ground and acidified to remove inOC (Tung & Tanner 2003) prior to analysis with a LECO CHN-900 auto analyser (LECO Corporation). For pore water sulphate determination, aliquots of the samples were diluted 100 times, and sulphate was measured on a Dionex System 14 ion

chromatograph (Dionex Corporation) with an AG4A guard column, an AS4A separator column and suppressed conductivity detection. A calibration line was constructed using known concentrations of a standard sulphate solution, from which the concentrations of the samples were determined (S. M. Harvey pers. comm.). Iron and manganese concentrations in pore water were determined using a PE 4300DV inductively coupled plasma-atomic emission spectrometer (Perkin Elmer Life & Analytical Sciences, Inc.). Calibrations were prepared from commercially available single-element standard solutions (CPI International) and were matrix matched to seawater with respect to sodium, potassium, calcium, magnesium and strontium. Pore water solutions were diluted by a factor of 20 in 5% v/v nitric acid solution and determined in axial mode.

Model description. The benthic–pelagic exchange was simulated using 2 models (Fig. 2):

(1) A particle-tracking and resuspension model, DEPOMOD (Cromey et al. 2002a), which predicts the flux of organic matter (OM) to the seabed due to the release of waste food and faeces; and

(2) A 1-dimensional early diagenesis model, hereafter termed EDM, implemented by means of the biogeochemical reaction network simulator (BRNS) (Regnier et al. 2003, Aguilera et al. 2005).
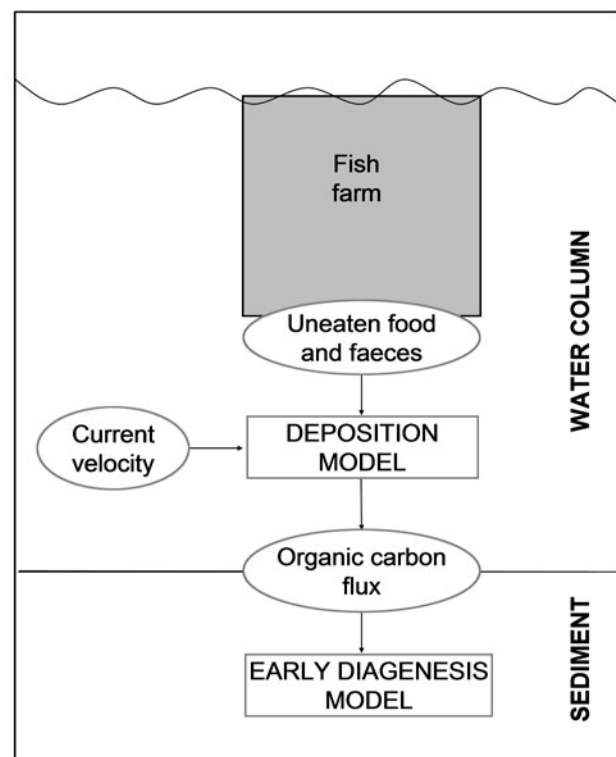

Fig. 2. Schematic representation of the integrated numerical models

The DEPOMOD-derived flux of OC from uneaten food and faeces released by the fish farm provides the boundary condition for the EDM.

The set up of the 2 coupled models involved 4 steps:

(1) The EDM was calibrated by comparing model output at steady state with the set of data collected at a site outside the fish farm deposition footprint (Stn B_C). This step provided an estimate of the background OC deposition fluxes;

(2) OC fluxes at 2 stations located near the fish farm were predicted by DEPOMOD (Stns B_{10} and B_{40});

(3) OC fluxes predicted by DEPOMOD were added to the background fluxes, and the EDM was then run for the transient state;

(4) Transient profiles predicted by the model were compared with data collected at the 2 stations located near the fish farm.

The study of the transient diagenesis involved 2 simulations: Run 1 for the 'nominal' conditions and Run 2 for a sensitivity test, carried out by varying the OC flux at the boundary of the EDM.

Deposition model. DEPOMOD is a local-scale, 2-dimensional model, which applies a Lagrangian method to simulate particle movement throughout the water column. Particles were advected using as input time series of water velocity at different depths, either recorded using current meters or estimated by means of a hydrodynamic model. Turbulence was represented as a random walk. Resuspension was related to critical values of current velocity at the seabed (Cromey et al. 1998, 2002b). As an output, see Fig. 2, the model provided 2-dimensional maps of OM flux at the seabed. The model was validated for Scottish sea lochs (Cromey et al. 2002a,b) and is currently used for regulatory purposes by the Scottish Environment Protection Agency (www.sepa.org.uk).

DEPOMOD predictions of carbon flux at the sediment–water interface (SWI) were obtained using a time series of farmed fish biomass from March to August 2006 (average 40×10^3 kg). Cage layout and husbandry data, provided by the fish farm company (www.scottishseafarms.com/), along with the other parameters used in the simulation are specified in Table 1. Hydrographic data had been collected at the site as part of regulatory requirements; summary statistics are presented in Table 2. All 3 meters (surface; mid-water; near-bed) showed residual water movement to the W-NW or SW, which is seaward. The residual is most pronounced on the surface layer due to freshwater runoff, and the tidal cycle is clearly defined with the near-bed meter, but less clear with the upper meters.

The carbon contents of feed and faeces were estimated on the basis of the references reported in Table 3. The water content of feed, usually set to the default value of 9% in DEPOMOD (Cromey et al. 2002a), was adjusted to 5.5%, see references in Table 3. No information on digestibility was available, and the default value of 85% was thus used.

The loss of carbon mass between the surface and sea bed was accounted for by determining, from settling velocities and depth at the site (27 m), the time necessary for the feed (5.4 min) and faeces (14.1 min) to settle. Carbon accounted for 27.7% of faecal mass using the 10 min immersion time from Chen et al. (2003). A 3% mass loss of carbon was used for feed pellets for a pre-conditioning time of 0 h (Stewart & Grant 2002). This represented an immediate loss in mass of the food pellet in the model and simulates loss of mass from dust and fragmentation.

Early diagenesic model. The EDM solves a set of partial differential equations (PDEs) describing the conservation of the mass of solid (Eq. 1) and dissolved

Table 1. Input data used for DEPOMOD model

Input data	Loch Creran	Data source
Grid cell size (m) – square grid	10	–
Number of cages	6	Farmer
Cage dimensions	Circular 22 m diameter; 14 m depth	Farmer
Number of current velocity data sets used	3	Provost (2001)
Height of moorings above sea bed (m)	25; 14; 2	Provost (2001)
Length of current velocity record (d); model time step (min)	18; 60	Provost (2001)
Months used for feed input	Mar–Aug 2006	–
Average biomass (kg)	40×10^3	Farmer
Specific feeding rate (SFR; % biomass d^{-1})	2.98	Farmer
Feed input (kg cage^{-1} d^{-1}):	190 (average value Mar–Aug 2006)	Estimated using SFR and biomass
Food settling velocity (cm s^{-1}; mean; SD)	Normal distribution (8.3; 1.5)	DEPOMOD default value
Faecal settling velocity (cm s^{-1}; mean; SD)	Normal distribution (3.2; 1.1)	DEPOMOD default value
Dispersion coefficients k_x; k_y; k_z (m^2 s^{-1})	0.1; 0.1; 0.001	DEPOMOD default value
Trajectory evaluation accuracy (s)	60	DEPOMOD default value
Mean tidal height (m)	1.8	Admiralty tide tables

Table 2. Summary statistics for hydrographic data for surface, mid-water and near-bed current using Interocean S4 electromagnetic current meters (Provost 2001)

Instrument depth	Max. speed (cm s^{-1})	Mean speed (cm s^{-1})	Residual direction (° True)	Residual speed (cm s^{-1})
Surface	33.0	8.2	279	3.5
Mid-water	24.9	4.5	224	0.3
Near-bed	24.8	5.1	285	0.6

(Eq. 2) species in a vertical sediment column (e.g. Berner 1980, Boudreau 1997), such that:

$$\frac{\partial[(1-\phi)C_s]}{\partial t} = -\frac{\partial[\omega(1-\phi)C_s]}{\partial z} + \frac{\partial}{\partial z}\left[D(1-\phi)\frac{\partial C_s}{\partial z}\right] + (1-\phi)\sum R \quad (1)$$

$$\frac{\partial\phi C_w}{\partial t} = -\frac{\partial\omega\phi C_w}{\partial z} + \frac{\partial}{\partial z}\left[D\phi\frac{\partial C_w}{\partial z}\right] + \phi\sum R \quad (2)$$

where C_s and C_w are, respectively, the concentration of solid and dissolved species, t denotes the time, z denotes the depth below the SWI, ϕ is sediment porosity, D is the total molecular diffusion plus bioturbation, D_b, ω is the sedimentation rate, and $\sum R$ represents the net rate of concentration change due to chemical and biological sources and sinks. The advection term includes burial and compaction; the diffusion term includes molecular and ionic diffusion, as well as bioturbation.

The reaction network includes 15 species and 17 reaction pathways (see Appendix 1) and is a modified version of the shelf case scenario described by van

Table 3. Literature review of feed and faecal properties from laboratory experiments. Carbon data are on a dry weight basis

	Value (%)	Source
Feed		
Carbon content	51.0	Stewart & Grant (2002), Fig. 5 (control)
	51.3	Petersen et al. (2005), Table 13
	55.5	Higgs & Stuchi (pers. comm.)
	49.6	Used as DEPOMOD input data[a]
Water content	5.2	Stewart & Grant (2002), Table 1
	5.9	Petersen et al. (2005), Tables 1 to 6
	5.5	Used as DEPOMOD input data
Faeces		
Carbon content	27.7	Chen et al. (2003), Table 3[b]
	23.7	Higgs & Stuchi (pers. comm.)
	27.6	Jusup (pers. comm.)[c]
	27.7	Cromey et al. (2002a,b)
Feed wasted	5	Cromey et al. (2002a,b)
Digestibility	85	Cromey et al. (2002a,b)

[a]Using the average of 51.0 and 51.3% and adjusted for 3% mass loss on immersion
[b]Standard diets, 10 min immersion time
[c]Using a digestibility of 78%

Cappellen & Wang (1996). Microbially mediated primary redox reactions (PRR) account for the main pathways of OC degradation, while secondary redox reactions (SRR) describe the most important processes of re-oxidation of the reduced products generated during OC oxidation.

The EDM accounted for all major metabolic pathways of OC decomposition, including methanogenesis, even though no direct evidence, for instance the presence of gas bubbles, was found at our study site, for the existence of this pathway. This decision was based on the consideration that this is a major mineralisation pathway in coastal environments subjected to a high OC load (Dale et al. 2008a).

According to Hargrave et al. (1993), Wildish et al. (1993) and Pitta et al. (1998), the modifications of sediment geochemistry induced by enhanced OC deposition are evident in dissolved nutrient and sulphide concentrations, particulate OC profiles and oxygen penetration depth. For these reasons, we neglected various precipitation/dissolution and adsorption reactions considered in some previous works (e.g. Jourabchi et al. 2005, Dale et al. 2009), which were shown to have a limited influence on the dynamics of the selected impacted geochemical indicators. The precipitation of FeS was included in the reaction network, due to its direct influence on the concentration of dissolved sulphides.

As far as phosphorus is concerned, processes of precipitation of phosphate minerals and fast and slow reversible sorption (recently modelled by Spiteri et al. 2007) were not considered. This choice was based on the hypothesis that the changes in the concentration of this species under high OM load are mainly governed by the mineralisation of OC.

OM mineralisation was modelled by means of a multi-G approach (Westrich & Berner 1984). Three pools of OM were included in the model, representing refractory OM (OM_1), labile OM (OM_2) and the salmon farm organic deposit (OM_3), respectively. The contribution of each microbially mediated decomposition pathway to the total carbon oxidation rate was modulated according to van Cappellen & Gaillard (1996), assuming a first-order dependency with respect to the electron donor (OM) concentration and a Michaelis-Menten relationship with respect to the terminal electron acceptor's concentration (Aguilera et al. 2005; see Appendix 2). Rates of the SRR follow a first-order dependency with respect to each of the reactants (e.g. van Cappellen & Wang 1996).

A fixed concentration was imposed at the upper boundary for all solutes, while a fixed flux was used for solids. A null-gradient condition was specified at the lower boundary for all chemical species. Even though the results presented here focus on the upper 10 cm layer, the physical domain of the model extended down to 40 cm depth, in order to minimise the computational artefacts generated from the null-gradient condition specified at the lower boundary. To our knowledge, no data on OM fluxes and reactive particulate Fe(III) and Mn(IV) fluxes at the upper boundary were available at our study site. These fluxes were therefore estimated during the calibration step, according to the strategy of inverse-use of the model proposed by van Cappellen & Wang (1996) and Wang & van Cappellen (1996) by minimising a goal function, Γ:

$$\Gamma = \sum_{i=1}^{n_{var}} \sum_{j=1}^{n_{obs}} \left(\frac{\hat{x}_{i,j} - x_{i,j}}{\bar{x}_i} \right)^2 \qquad (3)$$

where $\hat{x}_{i,j}$ and $x_{i,j}$ are, respectively, predicted and observed concentrations for the i-variable at the j-depth. The weight, $\bar{x}$, was introduced in order to normalise the contributions of state variables characterised by different concentration ranges.

The RTM simulations were carried out by means of the BRNS, a flexible modelling environment for 1-dimensional simulation (Regnier et al. 2003, Aguilera et al. 2005). In the BRNS, spatial domain and transport coefficients, chemical species involved, reaction stoi-chiometries, and kinetic and equilibrium parameters are specified by the user through a web-based interface, which automatically generates a set of Fortran routines to solve the specified reaction–transport equation (Regnier et al. 2002, 2003, Aguilera et al. 2005). A detailed description of the mathematical formulation of the BRNS is given by Aguilera et al. (2005). Model outputs provide concentrations, reaction rates and fluxes at any grid point of the discretised spatial domain.

All reaction rate coefficients of the SRR, the limiting concentrations of electron acceptors involved in the primary redox reactions and the apparent equilibrium constant for FeS precipitation were based on those found in the literature (see Table 4). Site-specific parameters characterising the depositional environment were estimated on the basis of experimental information available for the study site. Their values, as well as the values of the parameters defining the physical domain, are listed in Table 5. According to Jourabchi et al. (2005), the bioturbation coefficient exponentially decreases with depth. The value at SWI and the depth of the mixed layer were fixed according to the experimental values measured by Nickell et al. (2003) at 2 non-impacted stations located in the vicinity of the fish farm studied in this work. Depth-dependent sediment porosity values were derived from the interpolation of field data collected here (Fig. 3). The average sediment density was estimated from a set of field data collected at different sites nearby the fish farm. Burial velocity was set in accordance with work by Loh et al. (2002)

Table 4. Reaction-specific parameters in the diagenesic model. 1: Sources—Wang & van Cappellen (1996); 2: Jourabchi et al. (2005); 3: Canavan et al. (2006); 4: Berg et al. (2003)

Parameter name	Parameter value	Units	Description	Source
$O_{2\,lim}$	16.0×10^{-6}	mol l^{-1}	Limiting concentration for O_2	Mean value from 1,2,3,4
$NO_3^-{}_{lim}$	4.7×10^{-6}	mol l^{-1}	Limiting concentration for NO_3^-	Mean value from 1,2,3,4
$MnO_{2\,lim}$	13.3×10^{-6}	mol g^{-1}	Limiting concentration for MnO_2	Mean value from 1,2,3,4
$Fe(OH)_{3\,lim}$	87.0×10^{-6}	mol g^{-1}	Limiting concentration for $Fe(OH)_3$	Mean value from 1,2,3
$SO_4^{2-}{}_{lim}$	1180.0×10^{-6}	mol l^{-1}	Limiting concentration for SO_4^{2-}	Mean value from 1,2,3
k_7	1.2×10^7	(mol l^{-1})$^{-1}$ yr^{-1}	Kinetic constant for nitrification	Mean value from 1,2,3,4
k_8	3.3×10^8	(mol l^{-1})$^{-1}$ yr^{-1}	Kinetic constant for Mn^{2+} oxidation by O_2	Mean value from 1,2,3,4
k_9	4.2×10^8	(mol l^{-1})$^{-1}$ yr^{-1}	Kinetic constant for Fe^{2+} oxidation by O_2	Mean value from 1,2,3,4
k_{10}	3.7×10^7	(mol l^{-1})$^{-1}$ yr^{-1}	Kinetic constant for Fe^{2+} oxidation by MnO_2 kinetic constant	Mean value from 1,2,3,4
k_{11}	2.7×10^8	(mol l^{-1})$^{-1}$ yr^{-1}	Kinetic constant for sulphides oxidation by O_2 kinetic constant	Mean value from 1,2,3,4
k_{12}	2.3×10^4	(mol l^{-1})$^{-1}$ yr^{-1}	Kinetic constant for sulphides oxidation by MnO_2 kinetic constant	Mean value from 1,2,3,4
k_{13}	1.3×10^4	(mol l^{-1})$^{-1}$ yr^{-1}	Kinetic constant for sulphides oxidation by $Fe(OH)_3$ kinetic constant	Mean value from 1,2,3,4
k_{14}	7.1×10^6	(mol l^{-1})$^{-1}$ yr^{-1}	Kinetic constant for FeS oxidation by O_2 kinetic constant	Mean value from 1,2,3,4
k_{15}	1×10^{10}	(mol l^{-1})$^{-1}$ yr^{-1}	Kinetic constant for CH_4 oxidation by O_2	Mean value from 1,2,3
k_{16}	1×10^4	(mol l^{-1})$^{-1}$ yr^{-1}	Kinetic constant for CH_4 oxidation by SO_4^{2-}	Wang & van Cappellen (1996)
k_{17}	5×10^{-6}	(mol l^{-1}) yr^{-1}	Kinetic constant for FeS precipitation	Jourabchi et al. (2005)
K'_{FeS}	6.3×10^{-3}		Apparent equilibrium constant for FeS precipitation	Jourabchi et al. (2005)

Table 5. Definition of model physical domain and site-specific parameters (from Table 4). The bioturbation coefficient is a function of depth, z, is in centimetres: $D_b(z) = D_{b0} \cdot e^{(-z/\lambda)}$. OM: organic matter; SWI: sediment–water interface

Parameter	Value	Units	Reference
OM$_1$ rate constant, k_1	0.1	yr^{-1}	Derived from the Tromp et al. (1995) statistical model, using a site-specific burial velocity
OM$_2$ rate constant, k_2	0.0	yr^{-1}	–
OM$_3$ rate constant, k_3	1	yr^{-1}	deBruyn & Gobas (2004)
Acceleration factor for oxic processes, k_{acc}	25	–	Canavan et al. (2006)
C:N:P$_{OM1, OM2}$	80:8:1		Ansell et al. (1974), Tett et al. (1985)
C:N:P$_{OM3}$	70:8:1		Stewart & Grant (2002), deBruyn & Gobas (2004), Petersen et al. (2005)
Sediment porosity at SWI, φ_0	0.76	–	Present study
Sediment porosity at 10 cm depth, φ_∞	0.66		Present study
Shape coefficient for porosity, τ	0.3		Present study
Sediment density	1.43	g cm^{-3}	Harvey & Phillips (1994), Dean (2004), SEPA (2005)
Burial velocity, ω	0.1	cm yr^{-1}	Loh et al. (2002), Dean (2004)
Bioturbation coefficient at SWI, D_{b0}	78	cm^2 yr^{-1}	Nickell et al. (2003)
Attenuation coefficient, λ	1.5	cm	Nickell et al. (2003), Canavan et al. (2006)
Temperature	10.8	°C	Present study
Salinity	33.0		Present study
Time step	5.0×10^{-3}	yr	–
Max. depth	40	cm	–
Number of nodes	401	–	–

and Dean (2004). The OM degradation rate constant k_1 (0.1 yr^{-1}) of the labile OM$_1$ pool was determined by applying the global relationship proposed by Tromp et al. (1995). The value of the acceleration factor for aerobic decomposition, k_{acc}, was set in accordance with the value measured by Canavan et al. (2006) in a coastal freshwater lake. The ratio between the fluxes of OM$_1$ and OM$_2$ pools was set to 2:1, based on the evidence, reported by Loh et al. (2002), that Loch Creran sedi-

ments are rich in terrigenous highly refractory OM. The C:N:P ratio for OM$_1$ and OM$_2$ were set according to literature values listed in Table 5. No distinction was made between feed and faeces, based on the assumption that the elemental composition of faeces reflects that of the ingested diet. The OM$_3$ pool was considered separately in the model because the degradation rate constant for salmon farm deposits, k_3, is significantly higher than that of the OM$_1$ pool. k_3 was set to 1 yr^{-1}, in accordance with the rates of salmon farm-derived OM decomposition reported by deBruyn & Gobas (2004).

RESULTS

Deposition model

Fig. 4 shows the fluxes of farm-derived organic material, predicted by DEPOMOD. The model was forced using the values of fish biomass in the cages provided by the farmer for the period from March to August 2006 (Table 6). Mass balance calculations for the entire simulation revealed that 88% of OM$_3$ remains in the computational domain (400 m × 300 m) and 12% is exported. The deposition footprint is approximately elliptical and extends in a westerly direction from the salmon cages, which is consistent with the strong surface residual currents. The predicted deposition fluxes of OM$_3$ at Stns B$_{10}$ and B$_{40}$ are also reported in Table 6 and show that this flux is remarkably higher in the summer months, as a result of the rapid increase in fish biomass.
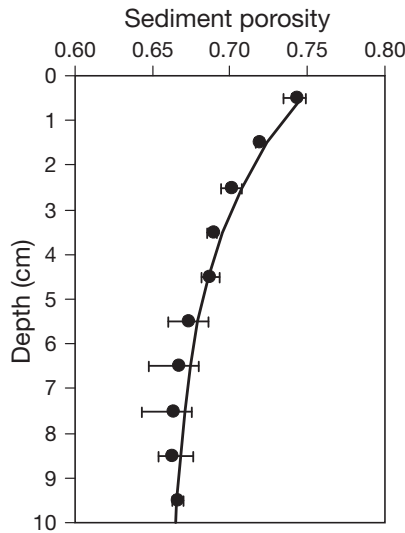

Fig. 3. Observed (solid dots) and modelled (solid line) depth-dependent porosity profile. The line was computed according to: $\varphi(z) = \varphi_\infty + (\varphi_0 - \varphi_\infty) \cdot e^{(-\tau \cdot z)}$. Parameter values are listed in Table 5, z is in centimetres, and whiskers represent the minimum to maximum range of observed value
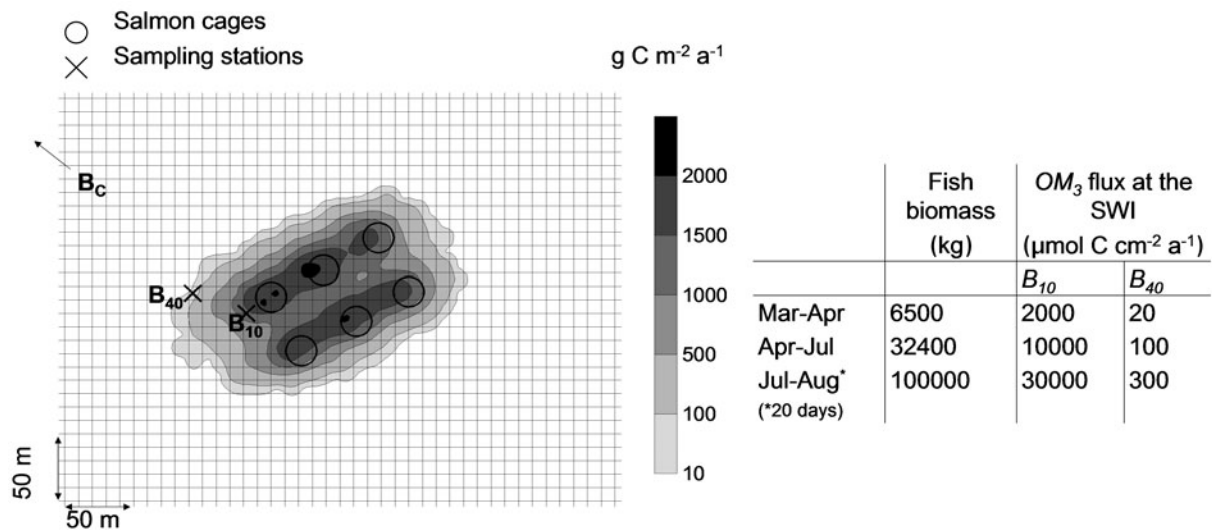
Fig. 4. Spatial distribution of carbon deposition flux predicted by DEPOMOD for the period from March to August 2006. OM: organic matter; SWI: sediment–water interface

EDM calibration

The model was calibrated under steady-state conditions by minimising the goal function, Eq. (3), against data collected at the pristine site, B_C. The optimal values for the solid deposition fluxes [$OM_T = OM_1 + OM_2$, Mn(IV) and Fe(III)] were found by comparing simulated and measured profiles of OC_T ($OC_1 + OC_2$), NH_4^+, SO_4^{2-}, DIP (dissolved inorganic phosphorus), Mn^{2+} and Fe^{2+}. The goal function was minimised over a range of OM_T fluxes comprised between 50 and 400 µmol C cm^{-2} yr^{-1}, in agreement with values reported by Ansell (1974) and Cronin & Tyler (1980) for Scottish sea lochs. As far as the fluxes of Fe(III) and Mn(IV) are concerned, no reference values were found for the study area; therefore, a broader range of values was explored, from 0.01 to 100 µmol cm^{-2} yr^{-1}. Fluxes of OM_T, Fe(III) and Mn(IV) resulting from the model calibration are reported in Table 7, while the observed and fitted model profiles are shown in Fig. 5. The 3 replicates show a significant variability, especially the nutrients. Simulated profiles of NH_4^+, DIP, SO_4^{2-} and Fe^{2+} con-

centrations are in overall agreement with field data, and, generally, within the range of observations. OC concentrations decrease only slightly with depth, corroborating the hypothesis that a substantial part of the OM is refractory. As far as the OC is concerned, the model slightly underestimated the concentration in the uppermost sediment layer. The model also largely underestimates Mn^{2+} in the upper layers of the sediment.

Table 7. Upper boundary conditions for the early diagenesis model. Values for solutes were constrained from observations. Solid flux values were estimated by fitting the model to the field data collected at Stn B_C. TS: total sulphides; DIP: dissolved inorganic phosphorus; OM: organic matter

Species	Upper boundary condition	Data source
Solute concentrations (µmol l^{-1})		
O_2	189	Rabouille pers. comm.
NO_3^-	4.7	Present study
NH_4^+	1.8	Present study
SO_4^{2-}	28×10^3	Present study
Mn^{2+}	3.34	Present study
Fe^{2+}	1.0	Present study
TS ($H_2S + HS^-$)	0	Rabouille pers. comm.
DIP	0.4	Present study
CH_4	0	Present study
Solid fluxes		
$OM_1 + OM_2$	120 (µmol cm^{-2} yr^{-1})	Model calibration
OM_1/OM_2	2 (–)	Derived from Loh et al. (2002)
MnO_2	1.0 (µmol cm^{-2} yr^{-1})	Model calibration
$Fe(OH)_3$	7.5 (µmol cm^{-2} yr^{-1})	Model calibration
FeS	0 (µmol cm^{-2} yr^{-1})	–

Table 6. Fish biomasses and OM_3 fluxes at Stns B_{10} and B_{40}. OM: organic matter; SWI: sediment–water interface

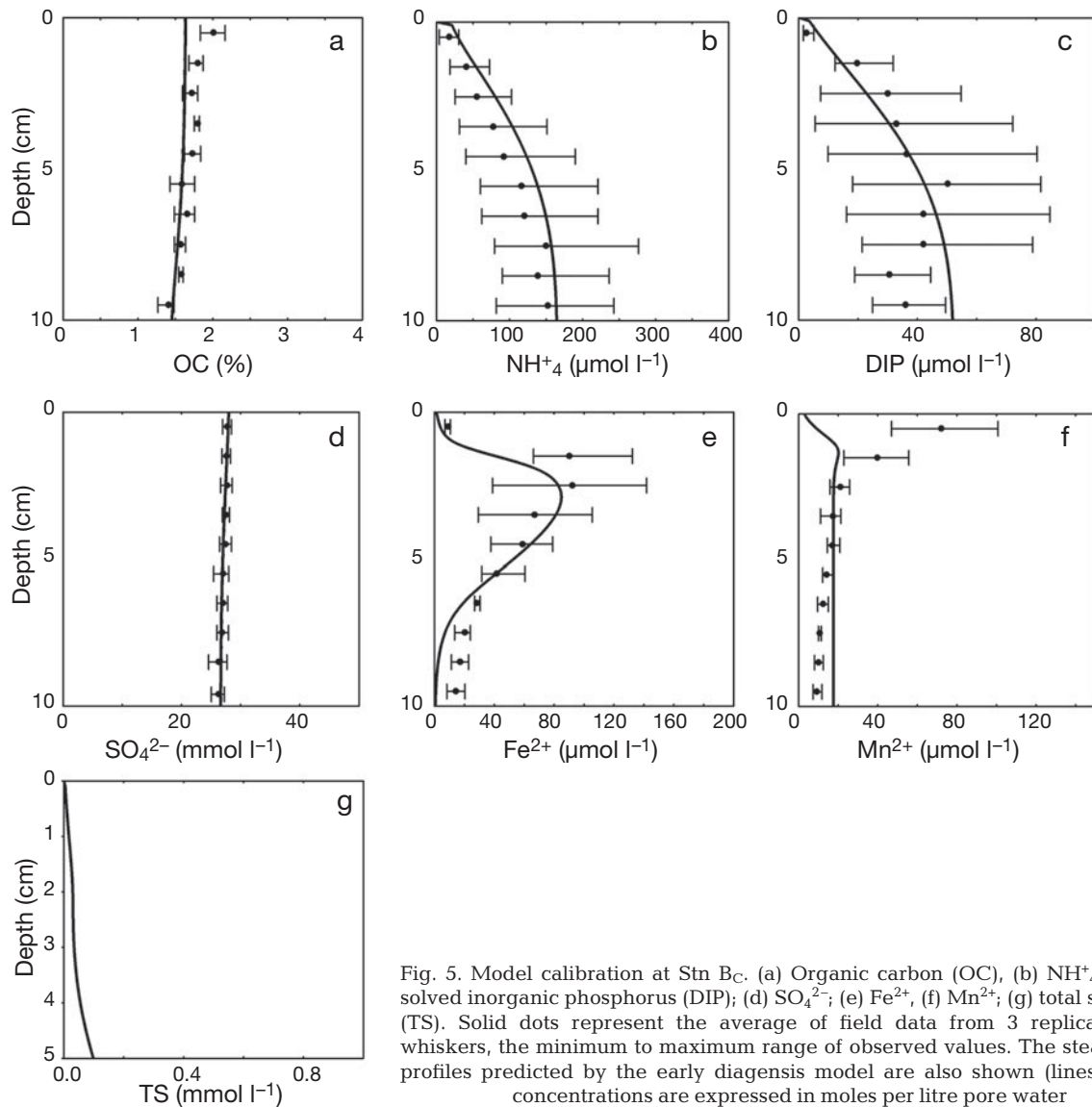|	Fish biomass (kg)	OM_3 flux at the SWI (µmol C cm^{-2} yr^{-1})	
		B_{10}	B_{40}
Mar–Apr	6500	2000	20
Apr–Jul	32400	10000	100
Jul–Aug[a]	100000	30000	300
[a]20 d			

Fig. 5. Model calibration at Stn B_C. (a) Organic carbon (OC), (b) NH^+_4; (c) dissolved inorganic phosphorus (DIP); (d) SO_4^{2-}; (e) Fe^{2+}, (f) Mn^{2+}; (g) total sulphides (TS). Solid dots represent the average of field data from 3 replicates, and whiskers, the minimum to maximum range of observed values. The steady-state profiles predicted by the early diagensis model are also shown (lines). Solute concentrations are expressed in moles per litre pore water

Depth-integrated rates of carbon mineralisation in the upper 40 cm of sediment are reported in Table 8; 40% of the carbon mineralisation occurs aerobically, the remaining being attributed to mainly sulphate reduction. The depth-integrated oxic mineralisation rate reported here falls within the range of 15 to 77 µmol C cm^{-2} yr^{-1}, derived by Canfield et al. (1993) from incubation experiments in coastal marine sediments. The rate of dissimilatory iron reduction is also similar to that found by Canavan et al. (2006).

EDM transient simulations

At Stn B_{40}, the average OM_3 flux predicted by DEPO-MOD (Fig. 4) is 0.1 mmol C cm^{-2} yr^{-1}, very close to the 0.12 mmol C cm^{-2} yr^{-1} of the natural OM_T flux reported in Table 7 for Stn B_C. Therefore, it is not surprising that the measured OC, NH_4^+, DIP and SO_4^{2-} concentration profiles are similar to those of the control station B_C (Fig. 6). Stn B_{40} is thus weakly impacted by the fish farm organic activities, and the variations in concentrations could thus also be due to the natural variability in sediment composition in the area. The transient evolution of concentration profiles triggered by fish farming are consequently only modelled at Stn B_{10}, where the average OM_3 flux is much larger (10 mmol C cm^{-2} yr^{-1}) and significant perturbations of the pristine biogeochemical conditions can, therefore, be expected.

To set-up Nominal Run 1, the following steps were carried out:

(1) The OM_3 flux predicted by DEPOMOD at Stn B_{10} was imposed as an additional source of labile OM for the EDM in addition to the deposition flux of OM_1 and OM_2;

Table 8. Simulated depth-integrated rates of organic carbon (OC) mineralisation through the various metabolic pathways at Stn B_C. See 'Results—EDM calibration' for the further details

Pathway	OC mineralisation rate (μmol C cm^{-2} yr^{-1})
Oxic respiration	32.1
Denitrification	1.2
Mn(IV) reduction	0.02
Fe(III) reduction	2.7
Sulphate reduction	44.0
Methanogenesis	0
Total	80.02

(2) The initial conditions of the system were set according to the steady-state results obtained at Stn B_C (Fig. 5);

(3) The model was run under transient conditions for 3 yr, and a snapshot was extracted at 0.5 yr, corresponding to a time for which field data were available.

For the transient simulation, the boundary conditions were constrained as follows. Based on the DEPOMOD results, the OM_3 flux was assumed to increase in 3 steps, according to Fig. 7b, and to

remain constant thereafter. A time variable bioturbation coefficient, linearly decreasing to zero within the 5 mo period was also imposed (Fig. 7), in agreement with the observations that sediments are azoic at Stn B_{10}. During the transient period, the burial rate was increased proportionally to the OM_3 fluxes. The effects of very high sulphate reduction rates on sulphate concentration within the topmost few millimetres of the sediment were accounted for by imposing a decreasing sulphate concentration at the upper boundary.

The transient results from the nominal run generally capture the main trends of the field data collected after 0.5 yr, with large increases in OC, NH_4^+ and DIP concentrations, and a marked drop in SO_4^{2-} concentrations (Fig. 8a to d). OC concentrations in the top 2 cm of the sediment reach values 8 times higher than at B_C, whereas the concentrations deeper in the sediment remain of comparable magnitude. Due to the mineralisation of large amounts of fish farm-derived labile OM, NH_4^+ and DIP concentrations at Stn B_{10} were approximately 10 times higher than those at Stn B_C (Fig. 5). Sub-surface maxima in nutrient concentrations were localised at around 5 cm depth, concomitant with a zone of sub-millimolar dissolved sulphate
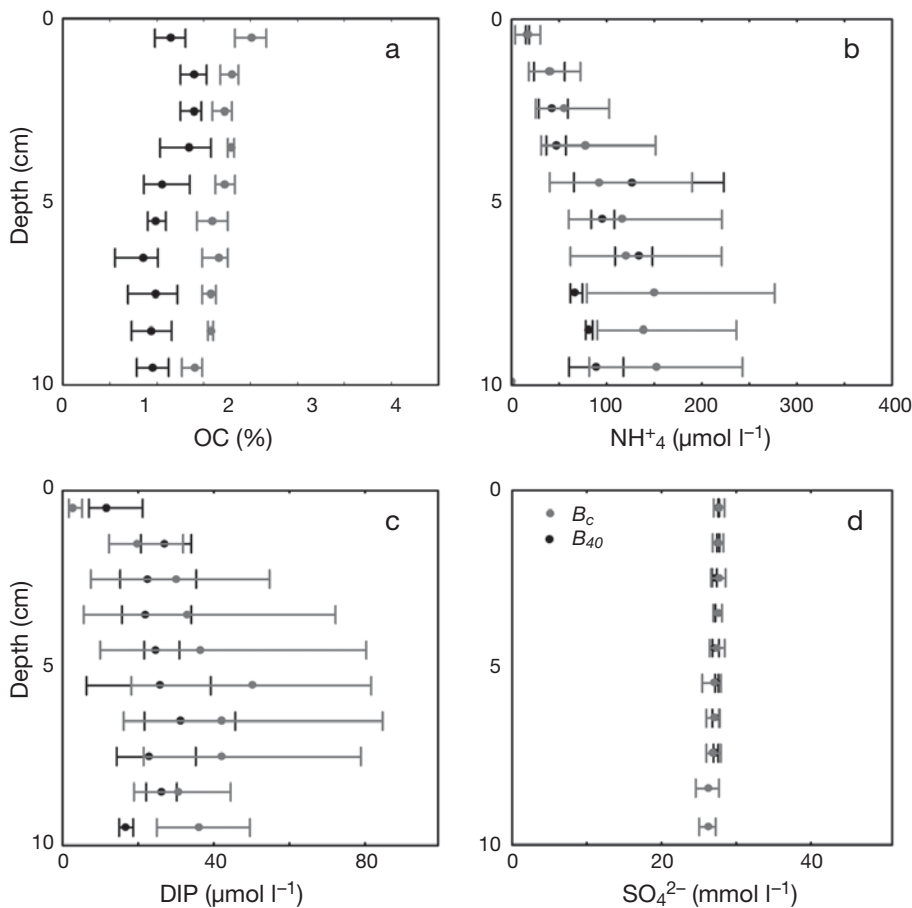

Fig. 6. Measured (a) organic carbon (OC), (b) NH_4^+, (c) dissolved inorganic phosphorus (DIP) and (d) SO_4^{2-} concentration profiles, at Stns B_C (grey) and B_{40} (black). Points represent average values, and whiskers, the minimum to maximum range of observed values. Solute concentrations are expressed in moles per litre pore water
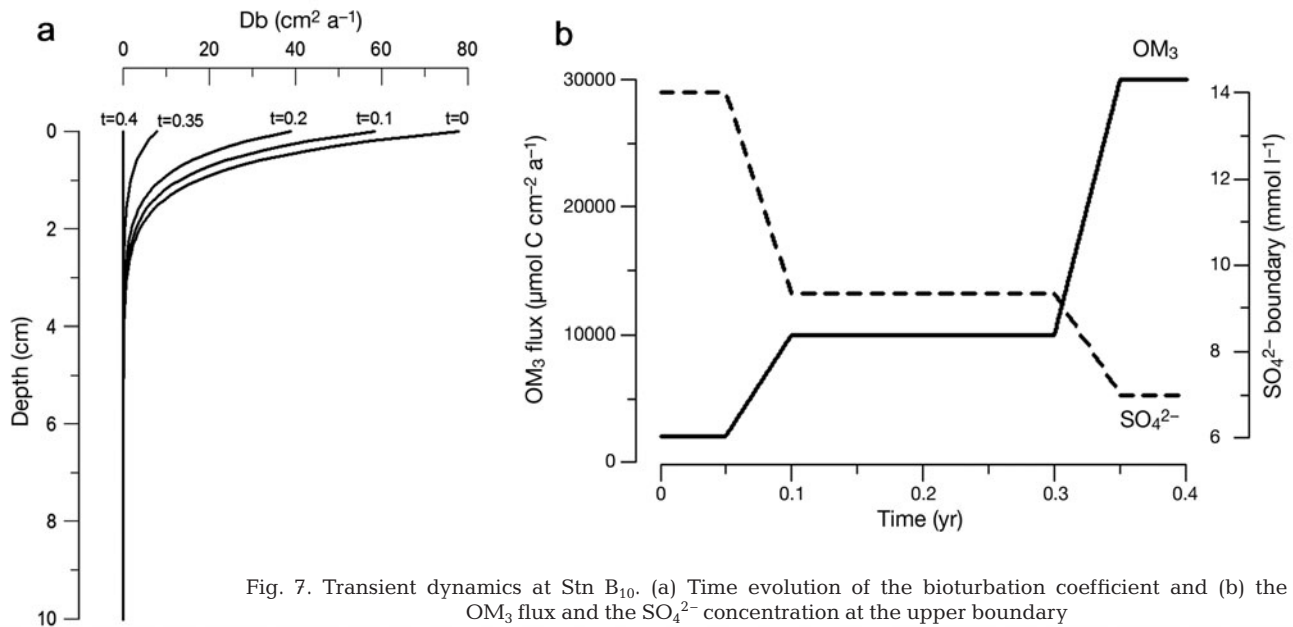
Fig. 7. Transient dynamics at Stn B_{10}. (a) Time evolution of the bioturbation coefficient and (b) the OM_3 flux and the SO_4^{2-} concentration at the upper boundary

concentrations. The depths of nutrient maxima predicted by the model were in good agreement with the field data, even though the DIP profile and NH_4^+ concentrations below 6 cm were slightly underestimated. Measured dissolved Fe^{2+} and Mn^{2+} concentrations were always very low, without any visible distinction between different replicates. The absence of dissolved Fe^{2+} was also predicted by the model, while model-predicted Mn^{2+} were slightly overestimated compared to field data, most likely because $MnCO_3$ precipitation was not included in the reaction network (see Appendix 1).

In Sensitivity Run 2, a variation of the OM_3 flux of ±50% was applied, according to the range of uncertainty of the DEPOMOD predictions (Cromey et al. 2002a). The grey lines in Fig. 8 show that the boundary condition variations induced remarkable changes in concentration profiles, especially for NH_4^+ and DIP. For these species, the model variability was higher than the variability in field data, as indicated by the black whiskers. Fig. 8d shows that SO_4^{2-} was also affected by changes in OM_3 fluxes and was totally consumed in the +50% OM_3 run at depths between 2 and 5 cm. In this case, the most important OM mineralisation pathway at 0.5 yr was no longer sulphate reduction, but methanogenesis.

The model was used for prognostic purposes, and the biogeochemical dynamics investigated over a much longer period of 3 yr until a new steady-state, consistent with an OM_3 flux of 30 mmol C cm^{-2} yr^{-1}, was reached. In this simulation, the OM_3 boundary flux was first set according to Fig. 7b, and then assumed to be constant in time, since no data on fish

biomass in the cages were available after 0.4 yr. Table 9 shows the evolution in depth-integrated pathways of OM oxidation. After 2 yr, the total depth-integrated rate of OM degradation reached 30 mmol C cm^{-2} yr^{-1}, corresponding to the imposed OM_1 + OM_3 fluxes at the SWI. At this stage, steady-state conditions were established with respect to the maximum deposition flux of OM_3. First, oxic degradation increased sharply, concomitant with the enhanced deposition of OM_3, then decreased slightly after 6 mo, due to the intense competition of SRR for oxygen by secondary redox reactions. Sulphate reduction rates showed also a rapid initial increase, which levels off after 6 mo. In relative terms, these 2 pathways contributed roughly equally to the total mineralisation rate during the increasing stages of OM_3 deposition. However, after 6 mo, methanogenesis became rapidly the most important pathway of OM decomposition and, after 2 yr, contributed 89% of the total mineralisation, sulphate reduction reaching barely 8% and oxic respiration 3%. The TS (total sulphides; H_2S + HS^-) flux through the SWI increased steadily and reached values as high as 1.5 mmol S cm^{-2} yr^{-1}. The progressive increase in the OM load and mineralisation also led to enhanced fluxes of DIP and ammonium through the SWI. This is in agreement with observations by Hargrave et al. (1993). The oxygen penetration depth (not shown) and the oxygen flux through the SWI did not change during the transient simulation period. The oxygen flux, on average, 1166 µmol O_2 cm^{-2} yr^{-1}, fell within the range recently measured by Dedieu et al. (2007) for a French lagoon (730 to 2190 µmol O_2 cm^{-2} yr^{-1}).
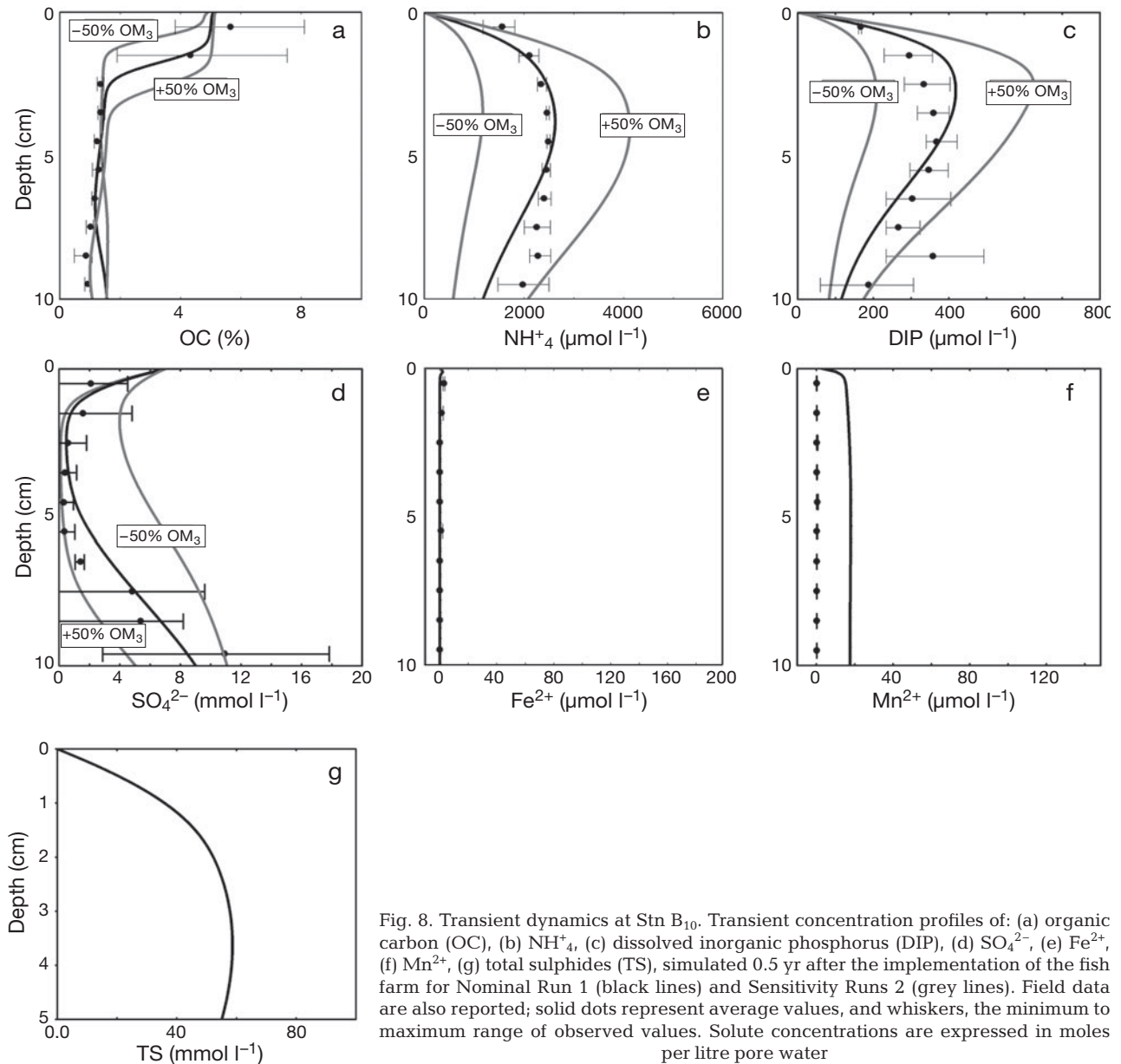
Fig. 8. Transient dynamics at Stn B_{10}. Transient concentration profiles of: (a) organic carbon (OC), (b) NH_4^+, (c) dissolved inorganic phosphorus (DIP), (d) SO_4^{2-}, (e) Fe^{2+}, (f) Mn^{2+}, (g) total sulphides (TS), simulated 0.5 yr after the implementation of the fish farm for Nominal Run 1 (black lines) and Sensitivity Runs 2 (grey lines). Field data are also reported; solid dots represent average values, and whiskers, the minimum to maximum range of observed values. Solute concentrations are expressed in moles per litre pore water

Table 9. Time evolution (in yr) of organic matter (OM) deposition flux, total depth-integrated rates of organic carbon oxidation, relative contribution of aerobic respiration, sulphate reduction and methanogenesis at Stn B_{10}. The fluxes of TS (total sulphides, H_2S + HS^-), nutrients (dissolved inorganic phosphorus [DIP], NH_4^+) and oxygen are also reported. The fluxes were computed by means of a third-order-accurate approximation of the concentration gradient (Boudreau 1997)

	0	0.25	0.5	1	2	3
OM flux (OM_1 + OM_3) [µmol C cm^{-2} yr^{-1}]	80	10080	30080	30080	30080	30080
Integrated rate [µmol C cm^{-2} yr^{-1}]	80	2559	8223	17698	30055	30070
Aerobic respiration [%]	40	61	33	11	4	3
Sulphate reduction [%]	55	39	29	13	8	8
Methanogenesis [%]	0	0	38	76	88	89
TS flux [µmol cm^{-2} yr^{-1}]	19	333	1002	1131	1307	1464
DIP [µmol cm^{-2} yr^{-1}]	4	19	45	96	184	271
NH_4^+ [µmol cm^{-2} yr^{-1}]	79	253	478	921	1690	2739
O_2 [µmol cm^{-2} yr^{-1}]	−1163	−1153	−1171	−1176	−1177	−1178

DISCUSSION

Calibration of the EDM

The calibration procedure provided estimates of the deposition fluxes of OM, $Fe(OH)_3$ and MnO_2 at the SWI of Stn B_C, for which field data were not available. A similar approach was previously adopted by Wang & van Cappellen (1996) and Canavan et al. (2006). Here, however, the calibration was performed using a goal function, instead of carrying out the adjustment of these forcings by visual inspection only. The systematic exploration of the entire space of possible boundary condition values represents a much more robust and reproducible way to calibrate a model.

The main objective of model calibration was to provide well constrained initial concentration profiles for the transient simulation corresponding to pristine conditions. We chose to compare the model results with the mean observed values, thus ignoring the variability between the 3 replicates. Therefore, model results are intended to provide an overall picture of the steady-state diagenesic processes and not to explain the observed discrepancies at each site. The dissolved ferrous iron, which was produced mainly by dissimilatory Fe^{3+} reduction (Reaction 4 in Appendix 1) was consumed by re-oxidation and FeS precipitation (Reactions 8, 9 and 12 in Appendix 1). Within the depth range of 6 to 10 cm, FeS precipitation dominated (results not shown) and might have been overestimated. The underestimated superficial concentration of Mn^{2+} predicted by the model could be due to rates of reoxidation through the overestimated aerobic pathway (Process 7 in Appendix 1), which outcompeted production, by Mn(IV) reduction, Fe^{2+} and TS reoxidation (Processes 3, 9 and 11 in Appendix 1). Even though the lack of fit in some portions of the profile for the trace metals is a potential drawback of setting the kinetic constants on the basis of literature values, their further calibration would be difficult without additional, reliable field information on the *in situ* kinetic rates, as well as on the concentrations of solid Mn(IV) and Fe(III) oxides.

Transient simulations

Soetaert et al. (1996) studied the diagenetic response of sediments subject to seasonally varying carbon deposition fluxes by means of a dynamic model. The model was run for 3 yr using as input the same annual time series of data, in order to achieve a periodic regime at the interannual time scale. A similar approach was recently used by Dale et al. (2008b) in anoxic sediments in Aarhus Bay, Denmark. In the study by Soetaert et al. (1996), the model parameters were calibrated to produce profiles that best fitted the experimental data collected at the same location in 2 subsequent years. Here, we propose a different strategy, calibrating first the model at one location under steady-state conditions and, then, using another independent dataset, testing the dynamic response of the system triggered by perturbation. This procedure can be regarded as an efficient way to assess model robustness, since it indicates that the model provides reasonable results in response to changes in the boundary conditions. This is a desirable property for a dynamic model, in particular if it is used to simulate transient scenarios (Canavan et al. 2006, Dale et al. 2008b).

The dynamic response of the EDM, importing from the steady-state conditions prevailing at Stn B_C, was investigated by adding the OM_3 deposition fluxes quantified by DEPOMOD to the natural contribution. The reliability of the transient results depends on the reliability of the model-predicted OC rain rates. The results from DEPOMOD were validated by means of sediment trap data, which were collected in similar sea loch environments (Cromey et al. 2002a); and the model is now used for regulatory purposes throughout Scotland. In addition, the results presented here (Stn B_{10}; Fig. 8) indicate that the coupled DEPOMOD and EDM models led to a reasonable description of the dynamics of early diagenesis under transient conditions, providing supplementary evidence that the estimate of the deposition flux is robust. The sensitivity test of EDM results to the changes in OM_3 deposition fluxes, furthermore, revealed that the diagenetic profiles were highly sensitive to this flux.

The field data collected at Stns B_C and B_{40} indicated similar concentrations of OC, SO_4^{2-}, DIP and NH_4^+ (Fig. 6). Modification in sediment geochemistry induced by enhanced OC deposition was much more obvious at Stn B_{10}, a result in agreement with previous studies (Hargrave et al. 1993, Wildish et al. 1993, Pitta et al. 1998). The transient simulation of OM deposition and diagenetic response captured the dominant variations of OC, DIP, NH_4^+, SO_4^{2-} and dissolved metal concentrations measured in the field. The coupled model also provided valuable information about the magnitude of fluxes of dissolved nutrients and TSs, which are required data for the implementation of sustainable aquaculture facilities. As regards model limitations, in cases of water bodies characterised by relatively high residence times, the transience of the SWI fluxes of oxygen and dissolved nutrients could, in principle, be simulated more accurately based on time-varying boundary conditions. This requires time series of data, from *in situ* on-line probes or from forecasts obtained by means of pelagic biogeochemical models. The uncertainty associated with this data may, in turn, de-

crease the robustness of the predictions of the diagenetic model. For this reason, the trade-off between costs and benefits associated with the introduction of time-variable boundary conditions should be carefully evaluated for each species considered.

Aquaculture-related model application

With respect to the aquaculture industry, the integrated model is useful: (1) to help support environmental impact assessment (EIA) and site selection studies, and (2) for the optimisation of farming densities and husbandry practices.

Wildish et al. (2001) investigated the cost-effectiveness of methods based, on the one hand, on macrofaunal community structure, and, on the other hand, on redox potential (Eh) and TS measurements. They concluded that the latter approach was superior to monitor the impact of fish farming. Even though macrofaunal measurements are currently adopted in most monitoring programs, these authors suggested that rapidity, ease and transferability were 3 major advantages of the geochemical approach. From a

prognostic perspective, the models presented here complement judiciously the sedimentary monitoring programmes, especially in the context of EIA and aquaculture site selection. For instance, Hargrave et al. (1997) ranked the sensitivity of 20 different indicators of organic enrichment under salmon net-pens in the Bay of Fundy (Canada) and proposed that TS flux, total CO_2 release and total O_2 uptake were the most sensitive indicators. In the future, the coupled model developed in the present study could help refine the choice of the most cost-effective indicators of organic enrichment.

Dissolved oxygen and TS were 2 cost-effective variables included in the model. The TS concentration at Site B_{10} increased dramatically from sub-millimole levels to concentrations >5 mmol l^{-1} within a few months (Figs. 5g & 8g), a level potentially toxic to benthic infauna. The predicted concentrations are, however, lower than the values of >100 mmol l^{-1} reported by Hargrave et al. (1993) at a salmon farm in the Bay of Fundy (Canada). The levels reported here are of the same order of magnitude as those measured in September 2006 by microelectrode profiling at a Loch Creran recovery site where salmon were reared until
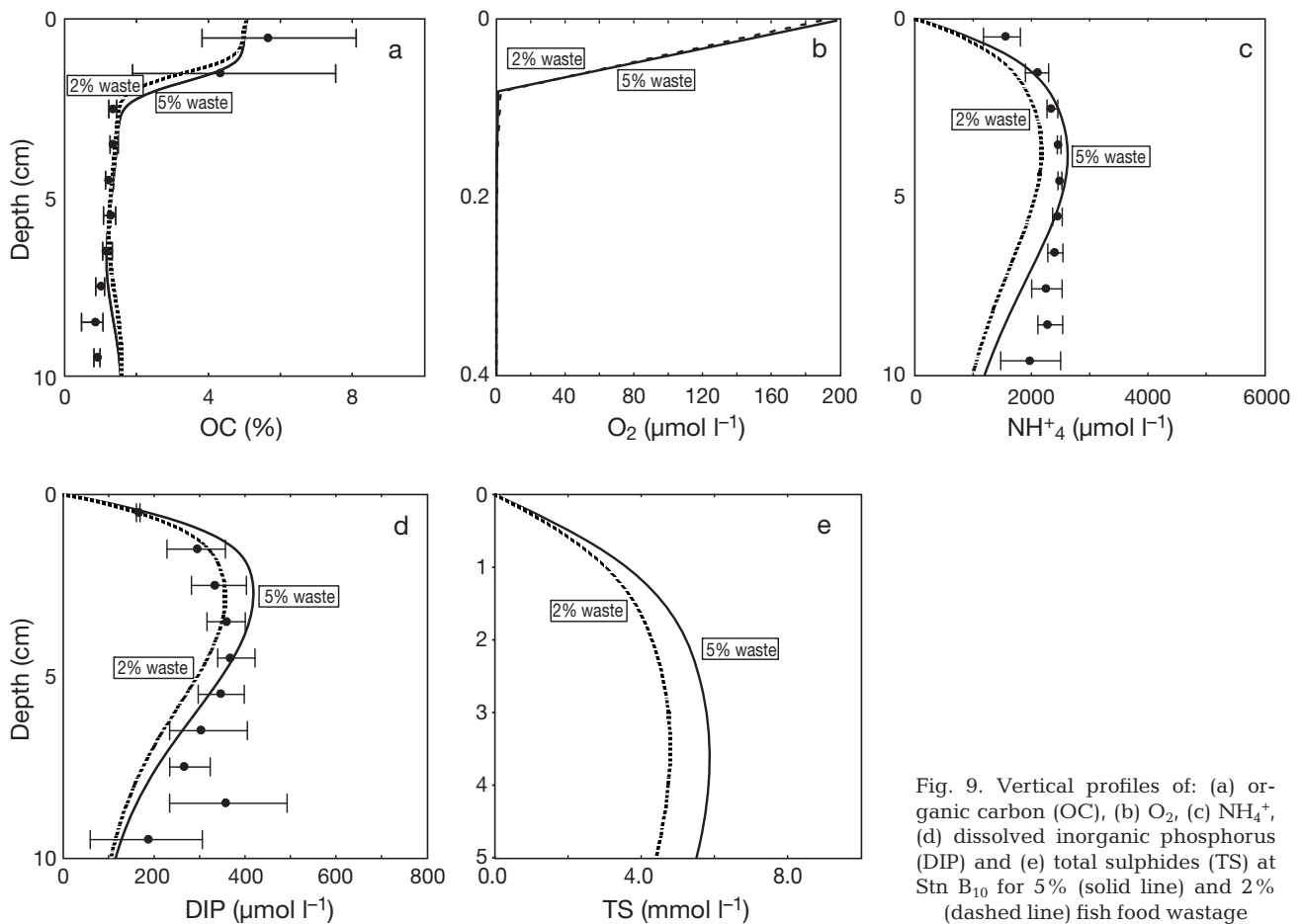

Fig. 9. Vertical profiles of: (a) organic carbon (OC), (b) O_2, (c) NH_4^+, (d) dissolved inorganic phosphorus (DIP) and (e) total sulphides (TS) at Stn B_{10} for 5% (solid line) and 2% (dashed line) fish food wastage

December 2005 (Rabouille pers. comm.). The low oxygen penetration depth predicted by the model, approximately 1 mm, is also in agreement with oxygen microprofiles reported elsewhere (see www.cobo.org.uk). In the future, the set of variables commonly measured in the field of aquaculture, e.g. OC and nutrients, could thus be extended to other geochemically based measurements, such as dissolved oxygen and sulphide microprofiles.

The coupled model can also support the estimation of husbandry practices. In this context, DEPOMOD was run again by assuming a lower percentage of fish food wasted, 2% instead of 5%, see data in Table 3; this lowered the OM_3 deposition fluxes at Stn B_{10}, from an average value of 10 to 8.5 mmol C cm^{-2} yr^{-1}. The EDM transient simulation was then repeated by imposing the lowered OM_3 flux at the upper boundary. Fig. 9 compares the resulting vertical profiles to those obtained under the assumption of a 5% of food wastage. The results reveal that dissolved nutrients and TS are the most sensitive variables, while OC and O_2 profiles remain essentially unaltered. The integrated model can thus help identify which geochemical variables are the most suitable to assess the impact of fish farming on the environment. It also provides a qualitative means to evaluate the effects of improved husbandry practices on water quality.

CONCLUSIONS

A model integrating deposition and early diagenesis of carbon has been developed and used in the context of aquaculture site selection, EIA and monitoring. On the basis of the model results, we have shown that the model provides a qualitative, robust means to evaluate the alteration of environmental conditions (nutrients, toxic compounds) as a result of fish farming activities. We advocate its use in combination with classical geochemical measures (e.g. NH_4^+, DIP) as a cost-effective means of EIA, but also together with alternative indicators, such as pore water oxygen and sulphide concentrations.

LITERATURE CITED

Aguilera DR, Jourabchi P, Spiteri C, Regnier P (2005) A knowledge-based reactive transport approach for the simulation of biogeochemical dynamics in Earth systems. Geochem Geophys Geosyst 6:Q07012

Ansell AD (1974) Sedimentation of organic detritus in Lochs Etive and Creran, Argyll, Scotland. Mar Biol 27:263–273

Aspila KI, Agemain H, Chau A (1976) A semi-automated method for the determination of inorganic, organic and total phosphorus in sediments. Analyst (Lond) 101:187–197

Barnett PRO, Watson J, Connelly D (1984) A multiple corer for taking virtually undisturbed samples from shelf, bathyal and abyssal sediments. Oceanol Acta 7:399–408

Berg P, Rysgaard S, Thamdrup B (2003) Dynamic modeling of early diagenesis and nutrient cycling: a case study in an arctic marine sediment. Am J Sci 303:905–955

Berner RA (1980) Early diagenesis: a theoretical approach. Princeton University Press, Princeton, NJ

Black KD (2001) Environmental impacts of aquaculture. Sheffield Academic Press, Sheffield

Boudreau BP (1997) Diagenetic models and their implementation: modeling transport and reactions in aquatic sediments. Springer, New York

Canavan RW, Slomp CP, Jourabchi P, van Cappellen P, Laverman AM, van den Berg GA (2006) Organic matter mineralization in sediment of a coastal freshwater lake and response to salinization. Geochim Cosmochim Acta 70:2836–2855

Canfield DE, Jørgensen BB, Fossing H, Glud R and others (1993) Pathways of organic carbon oxidation in three continental margin sediments. Mar Geol 113:27–40

Chen YS, Beveridge MCM, Telfer TC, Roy WJ (2003) Nutrient leaching and settling rate characteristics of the faeces of Atlantic salmon (*Salmo salar* L.) and the implications for modelling of solid waste dispersion. J Appl Ichthyol 19:114–117

Cromey CJ, Black KD, Edwards A, Jack IA (1998) Modelling the deposition and biological effects of organic carbon from marine sewage discharges. Estuar Coast Shelf Sci 47:295–308

Cromey CJ, Nickell TD, Black KD (2002a) DEPOMOD—modelling the deposition and biological effects of waste solids from marine cage farms. Aquaculture 214:211–239

Cromey CJ, Nickell TD, Black KD, Provost PG, Griffiths CR (2002b) Validation of a fish farm waste resuspension model by use of a particulate tracer discharged from a point source in a coastal environment. Estuaries 25:916–929

Cronin JR, Tyler ID (1980) Organic carbon in a Scottish sea loch. In: Albaiges J (ed) Analytical techniques in environmental chemistry. Pergamon Press, Oxford, p 418–426

Dale AW, van Cappellen P, Aguilera DR, Regnier P (2008a) Methane efflux from marine sediments in passive and active margins: estimations from bioenergetic reaction-transport simulations. Earth Planet Sci Lett 265:329–344

Dale AW, Aguilera DR, Regnier P, Fossing H, Knab NJ, Jorgensen BB (2008b) Seasonal dynamics of the depth and rate of anaerobic oxidation of methane in Aarhus Bay (Denmark) sediments. J Mar Res 66:127–155

Dale A, Brüchert V, Alperin M, Regnier P (2009) An integrated sulfur isotope model for Namibian shelf sediments. Geochim Cosmochim Acta 73:1924–1944

Dean R (2004) Biogeochemistry of metals in fish farm sediments. PhD thesis, UHI Millennium Institute, University of Aberdeen

deBruyn AMH, Gobas FAPC (2004) Modelling the diagenetic fate of persistent organic pollutants in organically enriched sediments. Ecol Modell 179:405–416

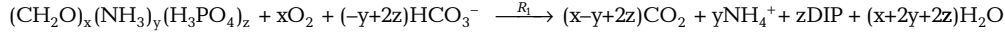Dedieu K, Rabouille C, Gilbert F, Soetaert K and others (2007) Coupling of carbon, nitrogen and oxygen cycles in sedi-

ments from a Mediterranean lagoon: a seasonal perspective. Mar Ecol Prog Ser 346:45–59

Edwards A, Sharples F (1986) Scottish sea lochs: a catalogue. Scottish Marine Biological Association, Oban

Gribble SD (2001) Robustness in complex systems. In: Proceedings of HotOS-VIII: 8th workshop on hot topics in operating systems, May 20 to 23, 2001, IEEE Computer Society, Elmau/Oberbayern

Hargrave BT, Duplisea DE, Pfeiffer E, Wildish DJ (1993) Seasonal changes in benthic fluxes of dissolved oxygen and ammonium associated with marine cultured Atlantic salmon. Mar Ecol Prog Ser 96:249–257

Hargrave BT, Phillips GA, Doucette LI, White MJ, Milligan TG, Wildish DJ, Cranston RE (1997) Assessing benthic impacts of organic enrichment from marine aquaculture. Water Air Soil Pollut 99:641–650

Harvey SM, Phillips CJ (1994) MAFF Project AE 0511—organic waste disposal in the marine environment. Dunstaffnage Marine Laboratory, Oban

Jourabchi P, van Cappellen P, Regnier P (2005) Quantitative interpretation of pH distributions in aquatic sediments: a reaction transport modeling approach. Am J Sci 305:919–956

Loh PS, Reeves AD, Overnell J, Harvey SM, Miller AEJ (2002) Assessment of terrigenous organic carbon input to the total organic carbon in sediments from Scottish transitional waters (sea lochs): methodology and preliminary results. Hydrol Earth Syst Sci 6:959–970

Luff R, Wallmann K (2003) Fluid flow, methane fluxes, carbonate precipitation and biogeochemical turnover in gas hydrate–bearing sediments at Hydrate Ridge, Cascadia Margin: numerical modeling and mass balances. Geochim Cosmochim Acta 67:3403–3421

Meysman F, Middelburg JJ, Herman P, Heip C (2003a) Reactive transport in surface sediments. I. Model complexity and software quality. Comput Geosci 29:291–300

Meysman F, Middelburg JJ, Herman P, Heip C (2003b) Reactive transport in surface sediments. II. Media: an object-oriented problem-solving environment for early diagenesis. Comput Geosci 29:301–318

Morel FMM, Hering JG (1993) Principles and applications of aquatic chemistry. John Wiley and Sons, New York

Naylor RL, Goldburg RJ, Primavera JH, Kautsky N and others (2000) Effect of aquaculture on world fish supplies. Nature 405:1017–1024

Nickell LA, Black KD, Hughes DJ, Overnell J and others (2003) Bioturbation, sediment fluxes and benthic community structure around a salmon cage farm in Loch Creran, Scotland. J Exp Mar Biol Ecol 285/286:221–233

O'Dell JW (ed) (1993) Method 350.1. Determination of ammonia nitrogen by semi-automated colorimetry (Revision 2.0, August 1993). Inorganic Chemistry Branch, Chemistry Research Division, Environmental Monitoring Systems Laboratory, Office of Research and Development, United States Environmental Protection Agency, Cincinnati, OH

Petersen SA, Sutherland TF, Higgs D (2005) Physical and chemical characterization of salmonid feed pellets. Can Data Rep Fish Aquat Sci 1159

Pitta P, Karakassis I, Tsapakis M, Zivanovic S (1998) Natural vs. mariculture induced variability in nutrients and plankton in the eastern Mediterranean. Hydrobiologia 391:179–192

Provost PG (2001) Current speed and meteorological measurements at a proposed fish cage site, Loch Creran. Data report prepared for Hydro Seafood GSP Ltd., Scottish Association for Marine Science, Oban

Regnier P, O'Kane JP, Steefel CI, Vanderborght P (2002) Modeling complex multi-component reactive-transport systems: towards a simulation environment based on the concept of a Knowledge Base. Appl Math Model 26:913–927

Regnier P, Slomp C, Jourabchi P (2003) Reactive transport modeling as a technique for understanding coupled biogeochemical processes in surface and subsurface environments. Neth J Geosci 82:5–18

SEPA (Scottish Environmental Protection Agency) (2005) Regulation and monitoring of marine cage fish farming in Scotland, Issue No. 2.3. Annex H. Issue date: 18 May 2005. Methods for modelling in-feed anti-parasitics and benthic effects. SEPA, Stirling. Available at: http://www.sepa.org.uk/water/water_regulation/regimes/aquaculture/marine_aquaculture/fish_farm_manual.aspx

Soetaert K, Herman PMJ, Middelburg JJ (1996) Dynamic response of deep-sea sediments to seasonal variations: a model. Limnol Oceanogr 41:1651–1668

Spiteri C, Slomp CP, Regnier P, Meile C, van Cappellen P (2007) Modelling the geochemical fate and transport of wastewater-derived phosphorus in contrasting groundwater systems. J Contam Hydrol 92:87–108

Stewart ARJ, Grant J (2002) Disaggregation rates of extruded salmon feed pellets: influence of physical and biological variables. Aquac Res 33:799–810

Strickland J, Parsons T (1972) A practical handbook of seawater analysis. Bulletin 167, Fisheries Research Board of Canada, Ottawa

Tett P, Wallis A (1978) The general annual cycle of chlorophyll standing crop in Loch Creran. J Ecol 66:227–239

Tett P, Heaney SI, Droop MR (1985) The Redfield ratio and phytoplankton growth rate. J Mar Biol Assoc UK 65:487–504

Thullner M, van Cappellen P, Regnier P (2005) Modeling the impact of microbial activity on redox dynamics in porous media. Geochim Cosmochim Acta 69:5005–5019

Thullner M, Regnier P, Van Cappellen P (2007) Modeling microbially induced carbon degradation in redox stratified subsurface environments: Concepts and open questions. Geomicrobiol J 24:139–155

Tromp TK, van Cappellen P, Key RM (1995) A global model for the early diagenesis of organic carbon and organic phosphorus in marine sediments. Geochim Cosmochim Acta 59:1259–1284

Tung JWT, Tanner PA (2003) Instrumental determination of organic carbon in marine sediments. Mar Chem 80:161–170

van Cappellen P, Gaillard JF (1996) Biogeochemical dynamics in aquatic sediments. In: Lichtner PC, Steefel CI, Oelkers EH (eds) Reactive transport in porous media: general principles and application to geochemical processes. Rev Mineral: 34, Mineralogical Society of America, Washington, DC

van Cappellen P, Wang YF (1996) Cycling of iron and manganese in surface sediments: a general theory for the coupled transport and reaction of carbon, oxygen, nitrogen, sulfur, iron, and manganese. Am J Sci 296:197–243

Wang Y, van Cappellen P (1996) A multicomponent reactive transport model of early diagenesis: application to redox cycling in coastal marine sediments. Geochim Cosmochim Acta 60:2993–3014

Westrich JT, Berner RA (1984) The role of sedimentary organic matter in bacterial sulfate reduction: the G-model tested. Limnol Oceanogr 29:236–249

Wildish DJ, Keizer PD, Wilson AJ, Martin JL (1993) Seasonal changes of dissolved oxygen and plant nutrients in seawater near salmonid net pens in the macrotidal Bay of Fundy. Can J Fish Aquat Sci 50:303–311

Wildish DJ, Akagi HM, Hamilton N, Hargrave BT (1999) A recommended method for monitoring sediments to detect organic enrichment from mariculture in the Bay of Fundy. Can Tech Rep Fish Aquat Sci 2286:1–34

Wildish DJ, Hargrave BT, Pohle G (2001) Cost-effective monitoring of organic enrichment resulting from salmon mariculture. ICES J Mar Sci 58:469–476
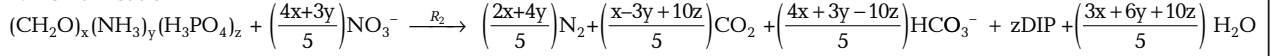
Appendix 1. Reaction network implemented in the early diagenesis model. The network is a simplified version of the one proposed by van Cappellen & Wang (1996). Reactions 1 to 5 were implemented separately for each organic matter fraction
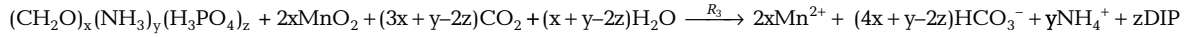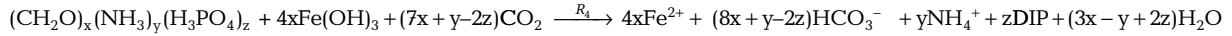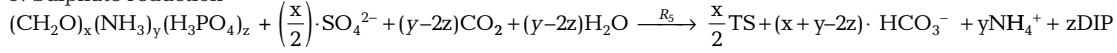
(a) Primary redox reactions

1. Oxic respiration

$$(CH_2O)_x(NH_3)_y(H_3PO_4)_z + xO_2 + (-y+2z)HCO_3^- \xrightarrow{R_1} (x-y+2z)CO_2 + yNH_4^+ + zDIP + (x+2y+2z)H_2O$$

2. Denitrification

$$(CH_2O)_x(NH_3)_y(H_3PO_4)_z + \left(\frac{4x+3y}{5}\right)NO_3^- \xrightarrow{R_2} \left(\frac{2x+4y}{5}\right)N_2 + \left(\frac{x-3y+10z}{5}\right)CO_2 + \left(\frac{4x+3y-10z}{5}\right)HCO_3^- + zDIP + \left(\frac{3x+6y+10z}{5}\right)H_2O$$

3. Mn(IV) reduction

$$(CH_2O)_x(NH_3)_y(H_3PO_4)_z + 2xMnO_2 + (3x+y-2z)CO_2 + (x+y-2z)H_2O \xrightarrow{R_3} 2xMn^{2+} + (4x+y-2z)HCO_3^- + yNH_4^+ + zDIP$$

4. Fe(III)reduction

$$(CH_2O)_x(NH_3)_y(H_3PO_4)_z + 4xFe(OH)_3 + (7x+y-2z)CO_2 \xrightarrow{R_4} 4xFe^{2+} + (8x+y-2z)HCO_3^- + yNH_4^+ + zDIP + (3x-y+2z)H_2O$$

5. Sulphate reduction

$$(CH_2O)_x(NH_3)_y(H_3PO_4)_z + \left(\frac{x}{2}\right)\cdot SO_4^{2-} + (y-2z)CO_2 + (y-2z)H_2O \xrightarrow{R_5} \frac{x}{2}TS + (x+y-2z)\cdot HCO_3^- + yNH_4^+ + zDIP$$

6. Methanogenesis

$$(CH_2O)_x(NH_3)_y(H_3PO_4)_z + (y-2z)H_2O \xrightarrow{R_6} \frac{x}{2}CH_4 + (\frac{x}{2}-y+2z)\cdot CO_2 + (y-2z)\cdot HCO_3^- + yNH_4^+ + zDIP$$
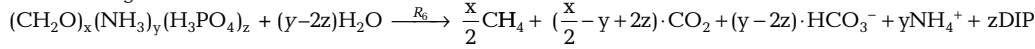
(b) Secondary redox reactions

7. Nitrification

$$NH_4^+ + 2O_2 + 2HCO_3^- \xrightarrow{R_7} NO_3^- + 2CO_2 + 3H_2O$$

8. Mn^{2+} oxidation by O_2

$$Mn^{2+} + \frac{1}{2}O_2 + 2HCO_3^- \xrightarrow{R_8} MnO_2 + 2CO_2 + H_2O$$

9. Fe^{2+} oxidation by O_2

$$Fe^{2+} + \frac{1}{4}O_2 + 2HCO_3^- + \frac{1}{2}H_2O \xrightarrow{R_9} Fe(OH)_3 + 2CO_2$$
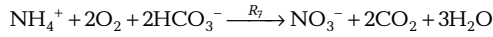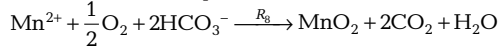
10. Fe^{2+} oxidation by MnO_2
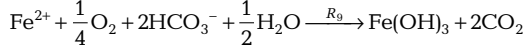
$$2Fe^{2+} + MnO_2 + 2HCO_3^- + 2H_2O \xrightarrow{R_{10}} 2Fe(OH)_3 + Mn^{2+} + 2CO_2$$

11. Sulphide oxidation by O_2

$$TS + 2O_2 + 2HCO_3^- \xrightarrow{R_{11}} SO_4^{2+} + 2CO_2 + 2H_2O$$
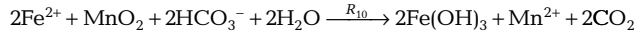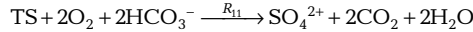
12. Sulphide oxidation by MnO_2

$$TS + 6CO_2 + 4MnO_2 + 2H_2O \xrightarrow{R_{12}} 4Mn^{2+} + SO_4^{2-} + 6HCO_3^-$$
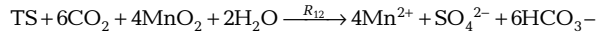
13. Sulphide oxidation by $Fe(OH)_3$

$$TS + 14CO_2 + 8Fe(OH)_3 \xrightarrow{R_{13}} 8Fe^{2+} + SO_4^{2-} + 14HCO_3^- + 6H_2O$$
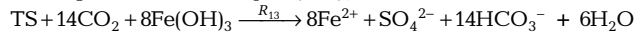
14. FeS oxidation by O_2

$$FeS + 2O_2 \xrightarrow{R_{14}} Fe^{2+} + SO_4^{2-}$$

15. CH_4 oxidation by O_2

$$CH_4 + O_2 \xrightarrow{R_{15}} CO_2 + H_2O$$

16. CH_4 oxidation by SO_4^{2-}

$$CH_4 + SO_4^{2-} + CO_2 \xrightarrow{R_{16}} H_2S + 2HCO_3^-$$
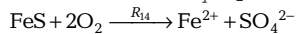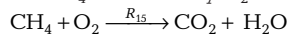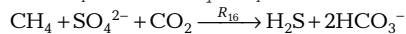
(c) Mineral precipitation

17. FeS precipitation

$$Fe^{2+} + TS + 2HCO_3^- \xrightarrow{R_{17}} FeS + 2H^+ + CO_2$$
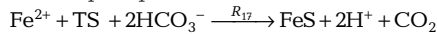
Appendix 2. Rate laws used in the early diagenesis model. Rates refer to the reactions listed in Appendix 1. f_i values were computed according to the formulation reported in Aguilera et al. (2005). $[H^+]$ concentration was assumed constant in time and fixed in accordance with the profiles reported by Jourabchi et al. (2005).

$R_1 = f_{o2} \cdot k_{OMk} \cdot [OM_k] \cdot k_{acc}$, with $k = 1, 2, 3$

$R_2 = f_{NO_2} \cdot k_{OMk} \cdot [OM_k] \cdot k_{acc}$, with $k = 1, 2, 3$

$R_3 = f_{MnO_2} \cdot k_{OMk} \cdot [OM_k]$, with $k = 1, 2, 3$

$R_4 = f_{Fe(OH)_3} \cdot k_{OMk} \cdot [OM_k]$, with $k = 1, 2, 3$

$R_5 = f_{SO_4} \cdot k_{OMk} \cdot [OM_k]$, with $k = 1, 2, 3$

$R_6 = f_{CH_4} \cdot k_{OMk} \cdot [OM_k]$, with $k = 1, 2, 3$

$R_7 = k_7 \cdot [NH_4^+] \cdot [O_2]$

$R_8 = k_8 \cdot [Mn^{2+}] \cdot [O_2]$

$R_9 = k_9 \cdot [Fe^{2+}] \cdot [O_2]$

$R_{10} = k_{10} \cdot [Fe^{2+}] \cdot [MnO_2]$

$R_{11} = k_{11} \cdot [TS] \cdot [O_2]$

$R_{12} = k_{12} \cdot [TS] \cdot [MnO_2]$

$R_{13} = k_{13} \cdot [TS] \cdot [Fe(OH)_3]$

$R_{14} = k_{14} \cdot [FeS] \cdot [O_2]$

$R_{15} = k_{15} \cdot [CH_4] \cdot [O_2]$

$R_{16} = k_{16} \cdot [CH_4] \cdot [SO_4^{2-}]$

$R_{17} = k_{17} \cdot \chi_{17} \cdot [\Omega_{FeS} - 1]$

$$\Omega_{FeS} = \frac{[Fe^{2+}] \cdot [TS]}{[H^+] \cdot K'_{FeS}} \qquad \begin{array}{l} \Omega_{FeS} > 1 \quad \chi_{17} = 1 \\ \Omega_{FeS} \leq 1 \quad \chi_{17} = 0 \end{array}$$